Hindawi
Advances in Materials Science and Engineering
Volume 2017, Article ID 2191659, 6 pages
https://doi.org/10.1155/2017/2191659

Research Article

Novel Preparation of Fe Doped TiO_2 Nanoparticles and Their Application for Gas Sensor and Photocatalytic Degradation

Sunil Babu Eadi,[1] Sungjin Kim,[1] Soon Wook Jeong,[1] and Heung Woo Jeon[2]

[1]*School of Advanced Materials & Engineering, Kumoh National Institute of Technology, 61 Daehak-Ro, Gumi 39177, Republic of Korea*
[2]*School of Electronic Engineering, Kumoh National Institute of Technology, 61 Daehak-Ro, Gumi 39177, Republic of Korea*

Correspondence should be addressed to Heung Woo Jeon; hwjeon@kumoh.ac.kr

Received 15 March 2017; Accepted 7 May 2017; Published 30 October 2017

Academic Editor: Fabrizio Pirri

The preparation of Fe doped TiO_2 is demonstrated as well as application for gas sensing and photocatalytic degradation. Fe doped TiO_2 nanopowder was prepared by the mechanochemical ball milling method. The results show the uniform doping of Fe in TiO_2 powder. The average size of the particle is observed to be ~28 nm. The H_2 gas sensor was fabricated using the Fe doped TiO_2 nanopowder and the effect of Fe doping on the sensing properties is investigated with various temperature ranges. The prepared Fe doped TiO_2 nanoparticles are also used to explore degradation properties of Rhodamine B dye under LED light.

1. Introduction

Titanium dioxide (TiO_2) is a well-known multifunctional metal oxide material because of its wide range of applications and benign properties such as stability and nontoxicity [1]. The wide range of uses of TiO_2 is due to its unique electronic and structural properties. TiO_2 exists in three main crystallographic forms: anatase, rutile, and brookite. However due to high band gap of TiO_2 (>3 eV) its optical application is limited to UV region of the electromagnetic spectrum [2]. Doping opens up the possibility of changing the electronic structure of TiO_2 nanoparticles, altering their chemical composition and optical properties. Much effort has been made by incorporating doping with metal ions, such as nickel, chromium, iron, vanadium, and zinc [3–7].

Iron metal ions have been considered as a suitable candidate, for doping owing to the fact that the radius of both Fe^{3+} (0.64 Å) and Ti^{4+} (0.68 Å) is similar in size. Therefore, it can be easily incorporated with the crystal lattice of TiO_2 [8]. One of the advantages of inclusion of Fe into TiO_2 lattice is its potential application in photocatalysis and hydrogen production due to reducing in the energy gap of TiO_2 and increasing the efficiency of absorbing visible light [9]. However, the application of Fe doped TiO_2 for gas sensing, especially hydrogen sensing, has still not been properly explored. It is also well recognized that doping Fe can improve the grain size, carrier concentration, and thermal stability of the TiO_2 sensor performance significantly. Furthermore, several researchers reported about the fabrication of Fe doped TiO_2 using the spin coating method Effendi and Bilalodin, reported the Fe doped TiO_2 powder using Titania and iron oxide as chemical precursors [10]. Kumar et al. reported the fabrication of Fe doped TiO_2 film by sol-gel technique for the application of gas sensor [11]. Othman et al., reported the Fe doped TiO_2 nanoparticles produced by MOCVD method for photocatalytic activity [12]. However, there are very few reports of preparing Fe doped TiO_2 nanoparticles by the mechanochemical ball milling method. Carneiro et al. studied the effect of Fe on TiO_2 powder on optical and photocatalytic properties [13].

In this work, we have developed Fe doped TiO_2 nanopowder using mechanochemical ball milling method. The effect of the ball milling procedure on Fe doping in TiO_2 is systematically studied. H_2 gas sensor was fabricated using the prepared powder and sensing properties are studied.

2. Experimental Procedure

Iron doped TiO_2 nanoparticles were prepared by ball milling of TiO_2 powders (TiO_2 P25) in a high-energy ball mill in the

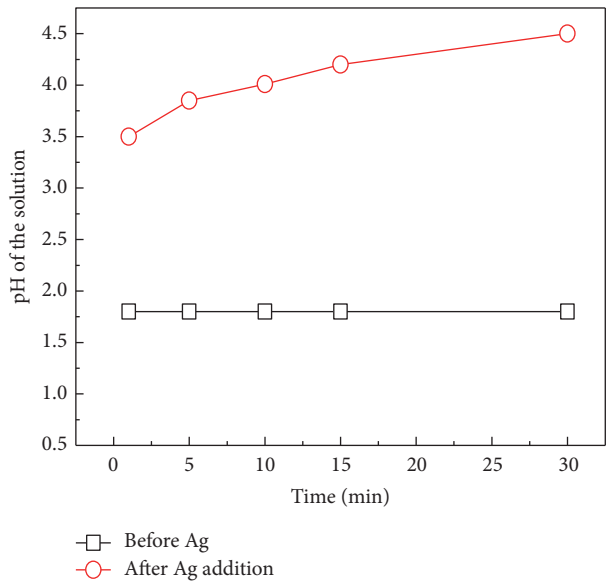

Figure 1: The pH variation during ball milling process.

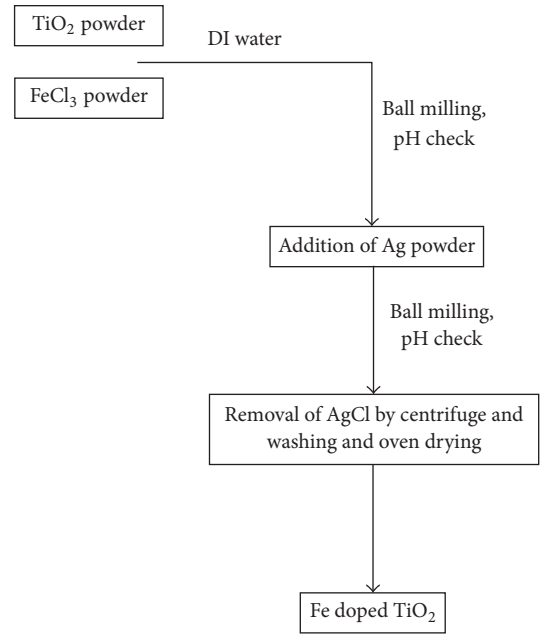

Figure 2: Flow chart for preparing Fe doped TiO_2.

presence of fine $FeCl_3$ powder using Al_2O_3 balls. The slurry was prepared by mixing TiO_2 powder and iron chloride in DI water in 1 : 5 ratio for 120 min at 1200 rpm. After 30 min the Ag powder was added in the slurry for the removal of unreacted $FeCl_3$. The slurry was monitored by pH meter. After reaction the slurry was washed with DI water and ethanol for removing the impurities. Finally, the powder was dried at 80°C in an open atmosphere.

3. Results and Discussion

Initially, the TiO_2 and $FeCl_3$ powders were mixed in DI water. The pH of the slurry changed to acidic medium with value 1.8. This indicates iron chloride dissolution in water and formation of iron hydroxide, as shown in (1) in the following:

$$FeCl_3\,(s) + H_2O\,(\text{excess}) \longrightarrow Fe^{3+}\,(aq) + 3Cl^-\,(aq) \quad (1)$$

$$2Fe^{3+}\,(aq) + 6H_2O \longrightarrow 2Fe\,(OH)_3\,(s) + 6H^+\,(aq) \quad (2)$$

The pH of the slurry remained steady for 30 min ball milling. To remove the Cl^- ions from the slurry Ag metal powder was added and the slurry was ball milled for another 30 min. During this time pH of slurry was increased gradually from 1.8 to 4.5 as shown in Figure 1. The experimental flow chart of fabrication of iron doped TiO_2 nanoparticles is shown in Figure 2. It is also noticed that amount of Fe dopant concentration in the TiO_2 slurry is very important for the controlling the pH and size of the particle. Increase in the concentration ratio of $FeCl_3$ to TiO_2 will lead to more lattice distortion in the crystal. It causes a decrease in the crystalline density, yielding an increase in the size of the nanoparticles. To characterize the surface area of the Fe doped TiO_2 nanoparticles BET measurement was used. The BET surface area obtained was 51.856 m^2/g and the total pore volume and average pore size were 0.462 cm^3/g and 357.246 Å, respectively. It was noted that the surface area

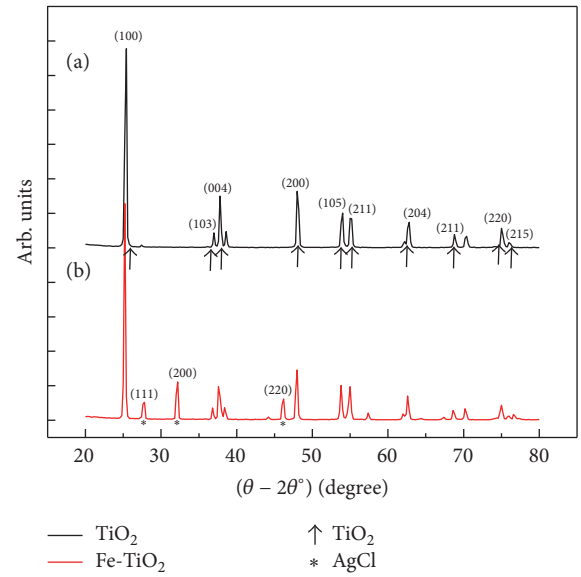

Figure 3: X-ray diffraction pattern of (a) pure TiO_2 and (b) iron doped TiO_2.

decreased with increasing in the annealing temperature of the powder. Table 1 shows the surface area, pore volume, and pore size of Fe doped TiO_2 at different annealing temperature.

Figure 3 shows the X-ray analysis of pure TiO_2 and synthesized Fe doped TiO_2 particles. The XRD profiles relieves the anatase phase (JCPDS number 84-1157) for pure TiO_2 and additional peaks of AgCl (JCPDS number 71-5209) for the doped sample as shown in the figure. All the peaks correspond to the (1 0 0), (0 0 4), (2 0 0), (1 0 5), (2 1 1), and (2 0 4) planes of anatase TiO_2. It is observed that the intensity of anatase phase in iron doped TiO_2 particles decreased with

Table 1: The surface area, pore volume, and pore size of Fe doped TiO_2 at different annealing temperature.

Sample name	BET surface area	Total pore volume	Average pore size
RT	51.856 m^2/g	0.462 cm^3/g	357.246 Å
400	50.514 m^2/g	0.455 cm^3/g	367.671 Å
500	43.288 m^2/g	0.338 cm^3/g	334.475 Å
600	23.132 m^2/g	0.071 cm^3/g	136.759 Å

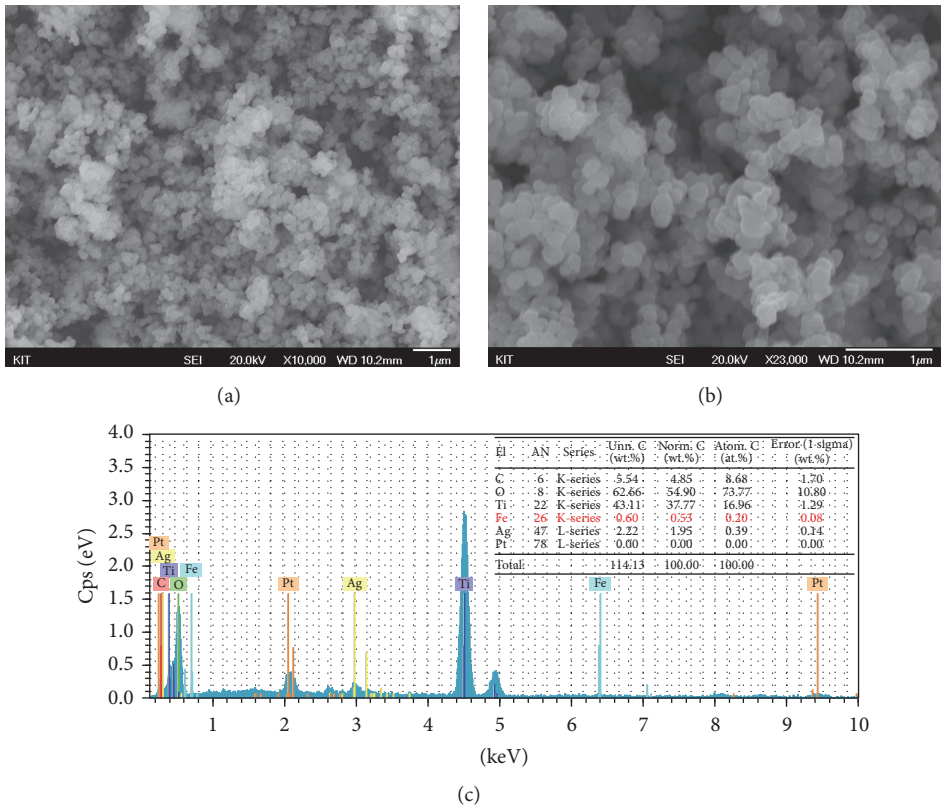

Figure 4: FESEM images of Fe doped TiO_2 (a) low magnification and (b) high magnification and (c) EDS spectrum table of the Fe doped TiO_2 particle.

insertion of Fe ions. However, in addition, it is worth noting that no crystalline phase attributed to iron oxide can be found in the XRD patterns.

One possible reason can be that the Fe^{3+} content in the Fe-TiO_2 is below the detection limit. The ionic radii of Ti^{+4} (0.68 Å) and Fe^{+3} (0.64 Å) are almost the same; hence there is a possibility of Fe ions occupying some of the lattice sites of TiO_2 [14]. The crystallite size of the Fe doped TiO_2 monodispersed nanoparticles is ~28 nm. Determined from the full-width at half maximum of the anatase peak by Scherrer's formula

$$Dp = \frac{K\lambda}{\beta \cos\theta}, \tag{3}$$

where Dp is average crystallite size, β is line broadening in radians, θ is Bragg angle, and λ is X-ray wavelength, respectively.

FESEM images of Fe doped TiO_2 powder obtained after annealing at 450°C for 1 hour are shown in Figures 4(a) and 4(b). The avg. diameters of the nanoparticles are ~28~30 nm. The nanoparticles are of uniform size and spherical shape. It is noticed that agglomeration of particles increases with the annealing temperature. Figure 4(c) shows the EDS spectrum of Fe doped TiO_2 nanoparticles. The peaks of titanium and iron can be clearly seen in the spectrum with a dotted spot in the FESEM image. From the spectrum table, we can see the Fe (at. % 0.53) in the TiO_2.

Gas sensing measurement was performed with sensor fabricated by Fe doped TiO_2 for the detection of H_2 gas. Figures 5(a) and 5(b) show schematic diagram of sensor fabrication and illustration of hydrogen sensor measurement instrument. The sensor was prepared by coating the paste of nanoparticles powder on precoated Pt electrode alumina substrate. Initially 500 ppm of H_2 reducing gas diluted with nitrogen was used as the source gas. The typical dynamic

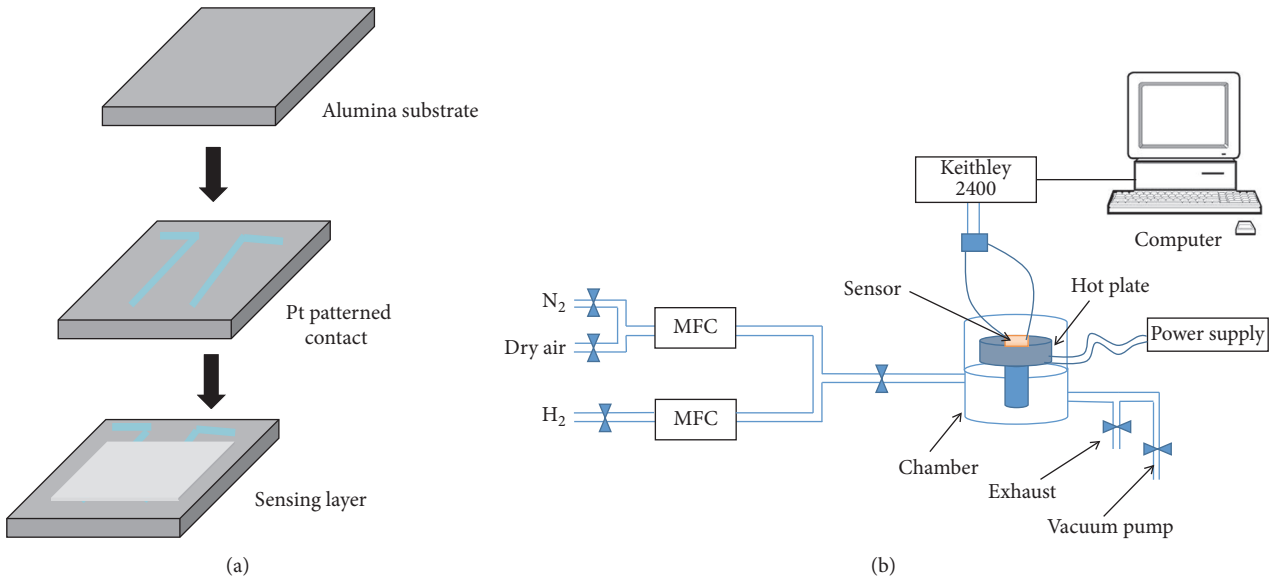

Figure 5: (a) Schematic diagram of sensor fabrication and (b) shows the schematic illustration of hydrogen sensor measurement instrument.

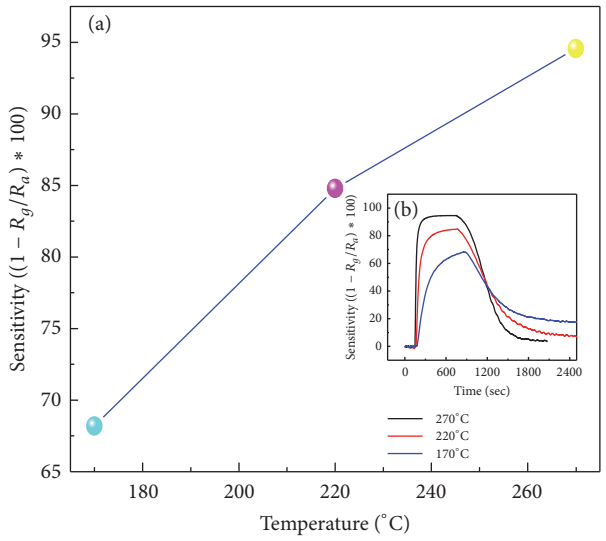

Figure 6: (a) Sensitivity plot at different operation temperatures 170, 220, and 270°C. (b) Dynamic responses from the sensor fabricated using Fe doped TiO_2 sample under the exposure of 500 ppm H_2.

responses of sensor upon exposure to 500 ppm H_2 (Figure 6(a)) diluted in nitrogen were measured at different operating temperature of 170, 220, and 270°C. TiO_2 shows typical gas sensing behavior of n-type semiconductor where first the resistance of the sensor increases the operating temperature and decreases upon exposure to the H_2 gas [15–17].

A plot of the sensitivity to 500 ppm H_2 concentration measured as a function of operating temperature is shown in Figure 6(b). The effect of temperature on sensitivity of sensor on the H_2 response was higher with an increase in temperature. A significant increase of the H_2 response was observed at 270°C. The sensitivities of 68.1, 84.7, and 94.5 were observed at temperatures of 170, 220, and 270°C, respectively. It is also noticed that at lower temperatures 170 and 220°C sensor took longer time to stabilize to normal state after H_2 gas is off. At 270°C sensor recovers fast due to rapid desorption from the surface of nanoparticles.

The H_2 gas sensing mechanism of the resistive sensor base on metal oxide semiconductors was proposed in previous reports [18–20]. In current measurement (temperature range 160°C < $T_{substrate}$ < 270°C), the O^- and O^{2-} oxygen ions are the dominant species on the surface of metal oxide semiconductors. The oxygen ions species extract electrons from the conduction of TiO_2. Thereby resistivity of the sensing layer increases and reaches steady state and when the H_2 gas is purged in; electrons are injected back to the conduction band thereby decreasing in resistance. In our case, sensing properties depend on the large surface area of the separated Fe doped TiO_2 particles, which provide more adsorption-desorption sites of gas molecules leading to improve the interaction between H_2 gas and adsorbed oxygen ions and thereby higher sensitivity was achieved.

The photodegradability of Rhodamine B dye solution was done using Fe doped TiO_2 powder. The solution was prepared by dissolving 0.2 g of Fe doped TiO_2 powder into 50 ml of 1 ppm concentration Rhodamine dye. Initially the solution was stirred for 30 min under dark to ensure complete surface adsorption of Rhodamine B onto the nanoparticles. After that LED white light was illuminated on the solution, for every 10 min samples were taken for checking the degradation property. Figure 7(a) shows the UV-Vis spectra of the dye solution with different interval time interval. The spectra data clearly demonstrates the photocatalytic efficiency of Fe doped TiO_2 powder in decolorization of Rhodamine B from pink to white under 60 min time interval. The gradual decrease

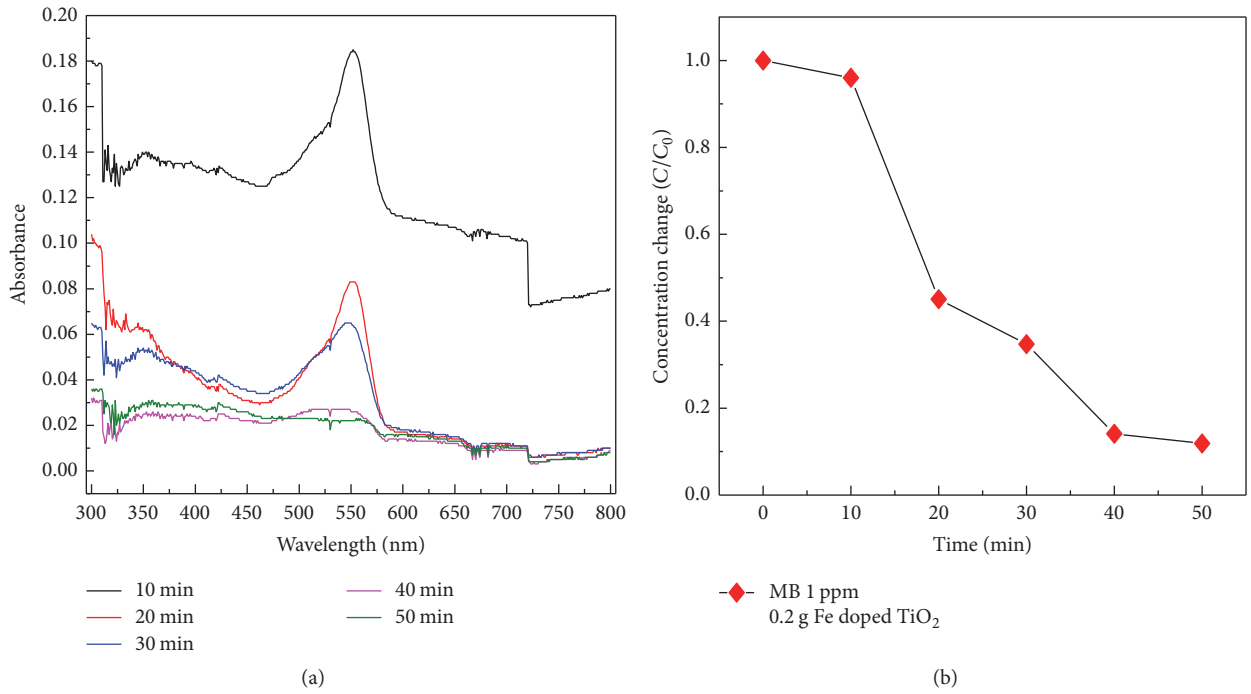

Figure 7: (a) UV-Vis spectra of the dye solution with different interval time and (b) shows the plot of concentration decreasing with time.

in the concentration ratio from initial to final decoloration is plotted in Figure 7(b). The photocatalytic mechanism of TiO_2 under UV light is well documented [21, 22]. Under the illumination of LED light, the pair of electron and hole released react with water and the electron-hole pairs migrate to the catalyst surface where they participate in redox reactions with adsorbed dye species. The holes (h^+) in valance band react with surface-bound H_2O to produce the hydroxyl radical and (e^-) in conduction band react with oxygen to generate superoxide radical anions. The formed hydroxyl radical ($^{\bullet}OH$) and superoxide radical anions ($O^{2\bullet-}$) degrade the pollutants in the photocatalytic oxidation processes. In our case, doping of Fe into TiO_2 enhances the electron-hole pair density thereby increasing the concentration of hydroxyl radical ($^{\bullet}OH$) and superoxide radical anions thereby showing efficient catalytical reaction.

4. Conclusions

In this study, Fe doped TiO_2 nanopowder is prepared by the mechanochemical ball milling method. The prepared powder was characterized by using field emission scanning electron microscope (FESEM) and X-ray diffraction studies. The results show the uniform doping of Fe in TiO_2 powder. The avg. size of the particle is observed to be 28 nm. The H_2 gas sensor fabricated using the Fe doped TiO_2 nanopowder shows high sensitivity of 86% and it was noticed that sensitivity depends on the temperature. Also the effect of Fe doping on photodegradation of Rhodamine B under LED light was investigated. The results show that doping helps in decreasing degradation time lower than 60 min.

Conflicts of Interest

The authors declare that they have no conflicts of interest.

Acknowledgments

This study was fully funded by Kumoh National Institute of Technology, Korea. The authors would like to acknowledge Ministry of Trade, Industry and Energy (MOTIE) Project 10063553 in 2016. They would also like to acknowledge WC 300 Project by Business for Global Cooperative R&D by Korea Small and Medium Business Administration in 2015.

References

[1] O. Ola and M. Mercedes Maroto-Valer, "Review of material design and reactor engineering on TiO_2 photocatalysis for CO_2 reduction," *Journal of Photochemistry and Photobiology C: Photochemistry Reviews*, vol. 24, pp. 16–42, 2015.

[2] Landmannm M., E. Rauls, and W. G. Schmidt, "The electronic structure and optical response of rutile, anatase and brookite TiO2," *Journal of Physics: Condensed Matter*, vol. 24, no. 19, 2012.

[3] A. Zaleska, "Doped-TiO_2: a review," *Recent Patents on Engineering*, vol. 2, no. 3, pp. 157–164, 2008.

[4] Y. Wang, H. Cheng, Y. Hao et al., "The photoelectrochemistry of transition metal-ion-doped TiO2 nanocrystalline electrodes and higher solar cell conversion efficiency based on Zn2+-doped TiO2 electrode," *Journal of Materials Science*, vol. 34, 1999.

[5] M. S. Jeon, W. S. Yoon, H. K. Joo, and T. K. Lee, "Preparation and characterization of a nano-sized Mo/Ti mixed photocatalyst," *Applied Surface Science*, vol. 165, no. 2-3, pp. 209–216, 2000.

[6] E. Traversa, M. L. Di Vona, P. Nunziante, S. Licoccia, T. Sasaki, and N. Koshizaki, "Sol-gel preparation and characterization of Ag-TiO2 nanocomposite thin films," *Journal of Sol-Gel Science and Technology*, vol. 19, no. 1-3, pp. 733–736, 2000.

[7] J. Moon, H. Takagi, Y. Fujishiro, and M. Awano, "Preparation and characterization of the Sb-doped TiO2 photocatalysts," *Journal of Materials Science*, vol. 36, no. 4, pp. 949–955, 2001.

[8] P. B. Nair, V. B. Justinvictor, G. P. Daniel et al., "Structural, optical, photoluminescence and photocatalytic investigations on Fe doped TiO_2 thin films," *Thin Solid Films*, vol. 550, pp. 121–127, 2014.

[9] R. D. S. Santos, G. A. Faria, C. Giles et al., "Iron insertion and hematite segregation on Fe-doped TiO 2 nanoparticles obtained from sol-gel and hydrothermal methods," *ACS Applied Materials & Interfaces*, vol. 4, no. 10, pp. 5555–5561, 2012.

[10] M. Effendi and Bilalodin, "Effect of doping Fe on TiO2 thin films prepared by spin coating method," *International Journal of Basic & Applied Sciences IJBAS-IJENS*, vol. 12, no. 2, 2012.

[11] M. Kumar, D. Kumar, and A. K. Gupta, "Undoped and Fe_ doped TiO2 thin films fabricated by sol-gel technique: an approach to gas sensing applications," *International Journal of Enhanced Research in Science, Technology & Engineering*, vol. 5, pp. 2319–7463, 2016.

[12] S. H. Othman, S. Abdul Rashid, T. I. Mohd Ghazi, and N. Abdullah, "3D CFD simulations of MOCVD synthesis system of titanium dioxide nanoparticles," *Journal of Nanomaterials*, vol. 2013, Article ID 123256, 11 pages, 2013.

[13] J. O. Carneiro, S. Azevedo, F. Fernandes et al., "Synthesis of iron-doped TiO_2 nanoparticles by ball-milling process: the influence of process parameters on the structural, optical, magnetic, and photocatalytic properties," *Journal of Materials Science*, vol. 49, no. 21, pp. 7476–7488, 2014.

[14] N. Nasrallaa, M. Yeganehb, Y. Astuti et al., "Structural and spectroscopic study of Fe-doped TiO2 nanoparticles prepared by sol-gel method," *Scientia Iranica*, vol. 20, pp. 1018–1022, 2013.

[15] G. F. Fine, L. M. Cavanagh, A. Afonja, and R. Binions, "Metal oxide semi-conductor gas sensors in environmental monitoring," *Sensors*, vol. 10, no. 6, pp. 5469–5502, 2010.

[16] G. Jiménez-Cadena, J. Riu, and F. X. Rius, "Gas sensors based on nanostructured materials," *Analyst*, vol. 132, no. 11, pp. 1083–1099, 2007.

[17] W. Guo, T. Liu, H. Zhang et al., "Gas-sensing performance enhancement in ZnO nanostructures by hierarchical morphology," *Sensors and Actuators B: Chemical*, vol. 166-167, pp. 492–499, 2012.

[18] N. M. Vuong, H. Jung, D. Kim, H. Kim, and S.-K. Hong, "Realization of an open space ensemble for nanowires: A strategy for the maximum response in resistive sensors," *Journal of Materials Chemistry*, vol. 22, no. 14, pp. 6716–6725, 2012.

[19] H. Gu, Z. Wang, and Y. Hu, "Hydrogen gas sensors based on semiconductor oxide nanostructures," *Sensors*, vol. 12, no. 5, pp. 5517–5550, 2012.

[20] C.-Y. Liu, C.-F. Chen, and J.-P. Leu, "Fabrication and CO sensing properties of mesostructured ZnO gas sensors," *Journal of The Electrochemical Society*, vol. 156, no. 1, pp. J16–J19, 2009.

[21] S. N. Frank and A. J. Bard, "Heterogeneous photocatalytic oxidation of cyanide and sulfite in aqueous solutions at semiconductor powders," *The Journal of Physical Chemistry*, vol. 81, 1484 pages, 1977.

[22] A. Fujishima and K. Honda, "Electrochemical photolysis of water at a semiconductor electrode," *Nature*, vol. 238, no. 5358, pp. 37-38, 1972.